Inorganic Chemistry

Article

pubs.acs.org/IC

π Donation and Its Effects on the Excited-State Lifetimes of Luminescent Platinum(II) Terpyridine Complexes in Solution

Lauren M. Hight, Meaghan C. McGuire, Yu Zhang, Matthew A. Bork, Phillip E. Fanwick, Adam Wasserman, and David R. McMillin*

Department of Chemistry, 560 Oval Drive, Purdue University, West Lafayette, Indiana 47907-2084, United States

Supporting Information

ABSTRACT: Introducing electron-donating groups extends the excited-state lifetimes of platinum(II)−terpyridine complexes in fluid solution. Such systems are of interest for a variety of applications, viz., as DNA-binding agents or as components in luminescence-based devices, especially sensors. The complexes investigated here are of the form $[Pt(4'\text{-X-T})Y]^+$, where 4′-X-T denotes a 4′-substituted 2,2′:6′,2″-terpyridine ligand and Y denotes the coligand. The π-donating abilities of −X and −Y increase systematically in the orders −NHMe < $-NMe_2$ < −(pyrrolidin-1-yl) and −CN < −Cl < −CCPh, respectively. The results presented include crystal structures of two new 4′-NHMe-T complexes of platinum, as well as absorption, emission, and excited-state lifetime data for nine complexes. Excited-state lifetimes obtained in deoxygenated dichloromethane vary by a factor of 100, ranging from 24 μs for $[Pt(4'\text{-pyrr-T})CN]^+$ to 0.24 μs for $[Pt(4'\text{-ma-T})Cl]^+$, where ma-T denotes 4′-(methylamino)-2,2′:6′,2″-terpyridine and pyrr-T denotes 4′-(pyrrolidin-1-yl)-2,2′:6′,2″-terpyridine. Analysis of experimental and computational results shows that introducing a simple amine group on the terpyridine and/or a π-donating coligand engenders the emitting state with intraligand charge-transfer (ILCT) and/or ligand−ligand charge-transfer (LLCT) character. The excited-state lifetime increases when the change in orbital parentage lowers the emission energy, suppresses quenching via d−d states, and encourages delocalization of the excitation onto the ligand(s). At some point, however, the energy is low enough that direct vibronic coupling to the ground-state surface becomes important, and the lifetime begins to decrease again.

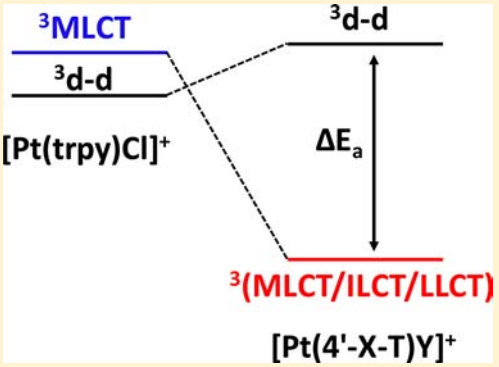

INTRODUCTION

Platinum(II) polypyridine complexes are planar d^8 systems capable of exhibiting intriguing luminescence properties.[1−4] Open access to the metal center permits Pt···Pt interactions in the solid state that often render luminescence signals sensitive to temperature and pressure variations as well as chemical exposure.[3−8] In the same way, encounters with a ground-state analogue can give rise to excimer emission in solution.[9] Solvent-induced quenching is another possibility when the orbital parentage of the emitting state exhibits significant metal-to-ligand charge-transfer (MLCT) character.[10] Rapid deactivation via thermally accessible d−d states can reduce excited-state lifetimes, not least in platinum(II) terpyridine complexes.[11] However, it is possible to mitigate the effect by introducing electronically active groups at either end of the 2-fold axis passing through the complex.[2−4] Results presented below reveal the effects of modifiying both ligands (Scheme 1).

More specifically, the π-donating strength of the ligand field increases with a change of coligand, −CN < −Cl < −CCPh, and/or the 4′-substituent on the terpyridine ligand, −NHMe < $-NMe_2$ < −(pyrrolidin-1-yl).

EXPERIMENTAL SECTION

Materials. The source for silver cyanide, K_2PtCl_4, 4′-chloro-2,2′:6′,2″-terpyridine (Cl-T), 1,5-cyclooctadiene (COD), diethanolamine, and routine salts, such as sodium trifluoromethanesulfonate (Na[OTf]), was Sigma-Aldrich. Laser dyes came from Exciton Inc., while the solvents used were from Mallinckrodt. $ZnBr_2$ and NaOH also came from Mallinckrodt as did $[Ru(bpy)_3]Cl_2$, where bpy denotes 2,2′-bipyridine. The complexes [Pt(dma-T)Cl]OTf and [Pt(dma-T)CN]OTf, where dma-T is 4′-(dimethylamino)-2,2′:6′,2″-terpyridine, and [Pt(pyrr-T)Cl]OTf and [Pt(pyrr-T)CN]OTf, where pyrr-T is 4′-(pyrrolidin-1-yl)-2,2′:6′,2″-terpyridine, were available from previous studies,[12,13] as was hydrated sodium tetrakis[3,5-bis-(trifluoromethyl)phenyl]borate (Na[TFPB]).[13]

Methods. Details for the syntheses of the 4′-(methylamino)-2,2′:6′,2″-terpyridine (ma-T) ligand and new platinum(II) complexes thereof follow next.

ma-T Ligand. The method employed is a variation on a published method for installing a methylamino group.[14] The first step entails

Scheme 1. Structures

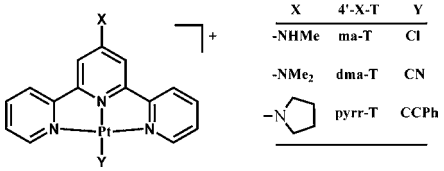

Received: February 21, 2013
Published: July 24, 2013

   dx.doi.org/10.1021/ic4004643 | Inorg. Chem. 2013, 52, 8476−8482

Table 1. Photophysical Data for [Pt(4′-X-T)Y]$^+$ Complexes in DCM at Room Temperature, Except as Noted

terpyridine	coligand	λ_{Abs}, nm	λ_{em}, nm	τ, μs 298 K	Φ 298 K	k_r, 10^4 s	τ_1, μs (f_1) 77 K
ma-T	CN	383, 399	497, 527	1.0	0.025	2.5	
	Cl	417, 432sh	532, 562	0.24	0.013	5.4	14.8 (0.65)
	CCPh	435, 464sh	576	4.8	0.12	2.5	12.9 (0.58)
dma-T	CN[16]	395, 415	524, 552	22	0.26	1.2	
	Cl	420, 444	535, 570, 635sh	1.9	0.11	5.8	18.6 (0.73)
	CCPh[34]	436, 457sh	567	5.6	0.20	3.6	15.8 (0.76)
pyrr-T	CN	402, 428	524, 557sh	24	0.15	0.63	
	Cl	423, 447	548, 583, 636sh	4.5	0.079	1.8	17.9 (0.81)
	CCPh[13]	440, 466	567	8.1[a]	0.073[a]	0.90	17.5 (0.74)

[a]Solvent was MeCN.

treating 0.500 g (1.9 mmol) of Cl-T with 6.0 mL of N-methylformamide and 0.526 g (5.0 mmol) of diethanolamine for 72 h at 150 °C in a thick-walled glass pressure vessel. Extracting the residue into DCM and treating with 0.470 g (2.1 mmol) of zinc bromide in methanol yielded Zn(ma-T)Br_2 as a solid after the addition of ether. Treatment of the zinc complex in 250 mL of DCM with 100 mL of 1.5 M NaOH(aq) resulted in the extraction of Zn(II) into the aqueous phase. Evaporation of the organic layer yielded the free ligand. ^{1}H NMR (300 MHz, $CDCl_3$): δ 8.69 (d, 2H), 8.6 (d, 2H), 7.82 (t, 2H), 7.63 (s, 2H), 7.3 (t, 2H), 4.5 (s,br, 1H), 3.0 (s, 3H). MS-ESI: (m +1)/z 262.80.

[Pt(ma-T)Y]OTf. The method reported by Annibale et al. yielded [Pt(ma-T)Cl]OTf from the reaction of the free ligand with Pt(COD)Cl_2.[15] Replacement of chloride by cyanide as the coligand was possible using a published double-exchange method.[16] The addition of tetrabutylammonium chloride to a solution of either triflate salt in acetone provided for isolation of the corresponding chloride salts. [Pt(ma-T)Cl]$^+$. ^{1}H NMR (300 MHz, $(CD_3)_2SO$): δ 8.48 (d, 2H), 8.32 (t, 2H), 8.01 (broad, 2H), 7.72 (t, 2H), 7.26 (broad, 2H), 2.88 (d, 3H), N−H resonance not resolved. The preparation of [Pt(ma-T)CCPh]PF_6 followed the method of Yang et al.[17] It involves charging 0.048 g (0.075 mmol) of [Pt(ma-T)Cl]PF_6 and 0.028 g (0.14 mmol) of CuI into a round-bottom flask and purging with N_2(g). The next step is to add 0.030 g (0.3 mmol) of phenylacetylene and 20 mL of dimethylformamide (DMF) while maintaining a nitrogen atmosphere. The addition of 0.030 g (0.3 mmol) of triethylamine promotes the reaction. After the reaction is over, the addition of excess KPF_6(aq) deposits the desired complex. Subsequent crystallization is possible by slow diffusion of ether into an acetonitrile solution of the complex.

[Pt(ma-T)CN]OTf·CH_3OH. Analysis Calculated for $C_{19}H_{18}F_3N_5O_4PtS$: C, 34.34; H, 2.73; N, 10.54%. Found: C, 34.53: H, 2.44; N, 10.38%.

[Pt(ma-T)CCPh]PF_6. Analysis Calculated for $C_{24}H_{19}F_6N_4PPt$: C, 40.98; H, 2.72; N, 7.96%. Found: C, 41.00: H, 2.87; N, 8.27%. [Pt(ma-T)CCPh]$^+$. ^{1}H NMR (300 MHz, $(CD_3)_2SO$): δ 8.87 (d, 2H), 8.50 (broad, 2H), 8.33 (t, 2H), 8.06 (broad, 2H), 7.73 (d, 2H), 7.42 (m, 2H), 7.34 (t, 2H), 7.28 (m,1H), 2.91 (s, br, 3H), N−H resonance not resolved.

Spectral Measurements. In most cases, measurement of room-temperature absorption, luminescence, and excitation spectra followed after extraction of the complex into dichloromethane with sodium tetrakis(3,5-trifluoromethylphenyl)borate (Na[TFPB]) as a solubility agent. The slit settings were 20 nm for all luminescence spectra obtained in DCM and 10 nm for excitation measurements, while an appropriate long-pass filter protected the detector from stray excitation light. The method of Parker and Rees[18] permitted determination of quantum yields with [Ru(bpy)$_3$]$^{2+}$ in deoxygenated acetonitrile as the standard (φ = 0.062).[19] The manufacturer provided instrumental emission intensity correction factors for the fluorimeter. Bubbling the samples with nitrogen for 20 min in a cuvette with a septum seal served to remove oxygen prior to quantum yield and lifetime determinations. Samples for cryostat measurements underwent four freeze−pump−thaw cycles. For lifetime measurements, the excitation wavelength was typically that of the CT absorption maximum or, rarely when the dye laser was not functioning, the intrinsic wavelength of the N_2 laser (337 nm). A previously described method allowed for extracting lifetimes from the decay profiles.[20]

Deuterium Exchange Studies. The addition of a small excess of DCl in CH_3OD to a solution of [Pt(4′-X-T)CN]Cl dissolved in the same solvent eventually yielded a yellow precipitate. Exposing the isolated solid to slightly less than one equivalent of Na[TFPB] in DCM allowed for extraction of the complex into solution. Filtration at room temperature and then a second filtration after volume reduction and cooling yielded a solution containing a deuterated complex. A comparison with the mass spectrum obtained with that of a control solution treated similarly with HCl in CH_3OH instead of DCl established that the complex exchanged one deuterium atom upon exposure to acid in CH_3OD. Because a second control experiment involving [Pt(pyrr-T)CN]$^+$ showed no evidence of deuterium incorporation, there is little doubt but that exchange occurred at the intended N−H position.

Instrumentation. The absorption spectrophotometer was a Varian Cary 100 instrument, and the spectrofluorimeter was a Varian Cary Eclipse. The ESI mass spectrometer was a Waters Micromass ZQ instrument. A previous publication describes the nitrogen-pumped dye laser and signal-acquisition equipment used for the excited-state lifetime determinations.[21] An Oxford Instruments DN1704 liquid-nitrogen-cooled system complete with an Oxford Instruments temperature controller was available for variable-temperature emission and lifetime measurements. The NMR spectrometer was a Varian Inova300. A CHI620A voltammetric analyzer served to record cyclic voltammograms. All electrochemistry involved a platinum disc working electrode, a silver/silver chloride in 3 M aqueous sodium chloride reference electrode, and a platinum wire as the auxiliary electrode.

Crystal Structures. A LINUX PC platform using SHELX-97 performed the refinements for crystallographic studies.[22] The diffractometers used were a Rigaku Rapid II equipped with confocal optics and a Nonius KappaCCD equipped with a graphite crystal, incident beam monochromator. The crystal of [Pt(ma-T)CN]-OTF·MeCN selected for structure determination was a red plate having approximate dimensions of 0.13 × 0.10 × 0.04 mm. As determined by Rigaku software product CrystalClear, the refined mosaicity was 1.05°, indicating poor crystal quality. The program used to determine the space group was XPREP.[22] The data collection was to a maximum 2θ of 133.2°. The solution program PATTY in DIRDIF99 solved the structure.[23] The refinement included hydrogen atoms, but the constraint was that each remain bound to a designated atom. Of the total of 9094 reflections collected, 3425 were unique and useful in the refinement; however, the calculation of R1 used only the 2823 reflections with $F_o^2 > 2\sigma(F_o^2)$. Table S1 summarizes the crystallographic data.

The crystal of [Pt(ma-T)Cl]OTF was a red needle of approximate dimensions of 0.63 × 0.15 × 0.10 mm. The program DENZO/SCALEPACK refined the mosaicity to be 0.95°, indicating moderate crystal quality, and the program XPREP established the space group. The method for solution of the structure was the same as above. Here, there were a total of 8698 reflections, of which 4084 were unique, and

dx.doi.org/10.1021/ic4004643 | Inorg. Chem. 2013, 52, 8476−8482

the 3867 reflections with $F_o^2 > 2\sigma(F_o^2)$ contributed to the calculation of R1. See Table S1 for more results.

Computational Details. Geometry optimization and adiabatic time-dependent density functional theory (TDDFT) excitation calculations are at the B3LYP level.[24,25] The quasi-relativistic Stuttgart/Dresden effective core potential MWB60[26] and its corresponding basis set apply to Pt, and the 6-311G**basis set applies to other atoms.[27] The optimized geometries of the first triplet excited states of dma-T and ma-T are obtained from spin-unrestricted SCF calculations. TDDFT calculations in these optimized geometries employ restricted Kohn−Sham references to facilitate comparison with the emission measurements. The polarizable continuum model (PCM) accounts for solvent effects.[28−30] A c-squared population analysis provided percentage contributions of fragmental AOs in the MOs.[31] The quantum chemistry package Gaussian 09 supplied the software for all calculations.[32]

RESULTS

Absorption and Emission Measurements. In keeping with results obtained with other platinum(II) polypyridine complexes,[2,3,33] the complexes studied herein all exhibit mainly intraligand absorptions at wavelengths below about 375 nm and charge-transfer (CT) absorptions at longer wavelengths, in the range of 375−475 nm. Absorption data compiled in Table 1 reveal that the energies of the CT band maxima vary with the 4′-amine substituent present on the trpy ligand, where trpy denotes 2,2′:6′,2″-terpyridine, as well as the coligand bound to platinum. Early experiments revealed that the counterion also influences the absorption spectrum of $[Pt(ma\text{-}T)Cl]^+$ in DCM solution. Figure S1 in the Supporting Information shows that the CT absorption exhibits more structure and occurs at slightly shorter wavelengths when the counterion is TFPB as opposed to the triflate ion. As the emission also shifts to shorter wavelengths when TFPB is present, it became the counteranion of choice for studies carried out in DCM.

The room-temperature absorption and emission spectra in Figure 1 pertain to $[Pt(ma\text{-}T)CN]^+$, $[Pt(dma\text{-}T)CN]^+$, and $[Pt(ma\text{-}T)CCPh]^+$, representative complexes from the series. As has been the case in previous studies,[2,34] partially resolved vibronic structure is sometimes evident in the CT emission spectrum, except if the coligand is CCPh. The results in Table 1 reveal that when the coligand is constant, the emission shifts to longer wavelength according to the strength of the electron-donating group on the trpy ligand, i.e., in the order ma-*T* < dma-*T* < pyrr-T. In the case of the CCPh complexes, however, the influence of coligand appears to be dominant because varying the trpy ligand has little effect on the emission maximum.

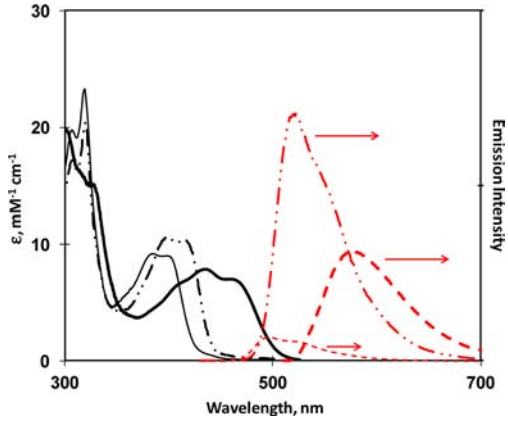

Figure 1. Absorption and emission spectra of representative $[Pt(4'\text{-}X\text{-}T)Y]^+$ complexes in DCM. Absorption spectra of $[Pt(ma\text{-}T)CN]^+$ (thin), $[Pt(dma\text{-}T)CN]^+$ (dot dash), and $[Pt(ma\text{-}T)CCPh]^+$ (thick). Corrected emission spectra (red) of $[Pt(ma\text{-}T)CN]^+$ (thin, dashed), $[Pt(dma\text{-}T)CN]^+$ (dot dash), and $[Pt(ma\text{-}T)CCPh]^+$ (thick, dashed). Areas of emission signals reflect relative quantum yields.

On the other hand, when the trpy ligand is constant, the emission maximum shifts to a longer wavelength as the coligand ranges from CN < Cl < CCPh, in keeping with the trend observed in the CT absorption bands. Data compiled in Table 1 reveal that $[Pt(ma\text{-}T)Cl]^+$ is the only complex in the series that exhibits a submicrosecond excited-state lifetime in deoxygenated DCM solution. The $[Pt(ma\text{-}T)Cl]^+$ complex also exhibits the lowest emission quantum yield of about 1.3%. At lower temperatures, however, the lifetime of $[Pt(ma\text{-}T)Cl]^+$ lengthens considerably. Equation 1 models the behavior with $\Delta E_a = 1830\ cm^{-1}$ and $A = 2.7 \times 10^{10}\ s^{-1}$.

$$\tau^{-1} = \tau_0^{-1} + A\ e^{-\Delta E_a/kT} \quad (1)$$

Both the $[Pt(dma\text{-}T)CN]^+$ and $[Pt(pyrr\text{-}T)CN]^+$ systems exhibit much longer room-temperature excited state lifetimes of 22 and 24 μs, respectively. The emission quantum yields are correspondingly higher, too. At platinum concentrations of less than about 10 μM, self-quenching is minimal, particularly when the lifetime is relatively short to begin with. However, at higher concentrations self-quenching is evident with $[Pt(pyrr\text{-}T)CCPh]^+$, where $k_q = 1.8 \times 10^9\ M^{-1}\ s^{-1}$. N−H deuteration has no measurable impact on the lifetime of $[Pt(ma\text{-}T)CN]^+$. In a rigid glass at 77 K, the photoexcited states of the complexes under investigation tend to exhibit biphasic decay, as has been reported previously.[34] Table 1 includes the lifetime of the dominant, longer-lived component of the decay observed in a DME glass, along with the fractional contribution to the total signal amplitude. See the Supporting Information (Table S2) for more details.

Data in the text of the Supporting Information confirm that electron-donating substituents shift ligand-based reduction in the cathodic direction, as reported for related systems.[35] The presence of an amine substitutent shifts the first reduction potential by about 280 mV more negative, while the shift is about half as large for the second reduction.

Crystal Structure of [Pt(ma-T)Cl]OTf. Figure 2 is a thermal-ellipsoid view of the complex complete with an atom-numbering scheme. The caption provides a list of bond angles and bond distances which are similar to those of related platinum terpyridine complexes.[2,3,36] In terms of the methyl-amino substituent, the C17−N19−C20 plane makes a dihedral angle of 0.58° with respect to the best plane through the carbon and nitrogen atoms of the trpy ligand. The corresponding dihedral angle is 5.9° in a related dma-T derivative.[12] The chloride complexes stack as dimers along the *b* direction with a Pt···Pt spacing of 3.86 Å, too long for significant metal−metal interaction.[36,37] As in a $[Pt(dma\text{−}T)CN]^+$ structure,[12] the packing is not exactly head to tail, as the Cl−Pt−Pt−Cl torsion angle is 125.22° rather than 180°. Within a dimer, the mean planes through the platinum complexes are, however, mutually parallel.

Crystal Structure of [Pt(ma-T)CN]OTf·CH_3CN. A thermal-ellipsoid view of the complex along with an anion appears in Figure 3, which also reveals the atom-numbering scheme. The caption includes a list of selected bond angles and bond lengths as before. The dihedral angle relating the best plane through the carbon and nitrogen atoms of the trpy ligand and

dx.doi.org/10.1021/ic4004643 | Inorg. Chem. 2013, 52, 8476−8482

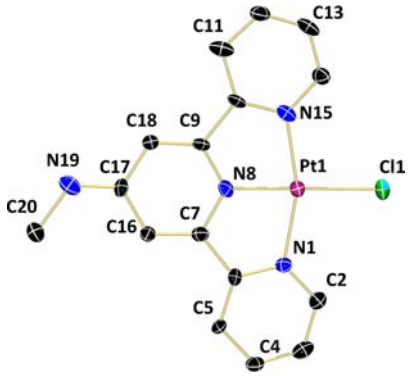

Figure 2. The molecular structure of a representative cation of [Pt(ma-T)Cl]OTf with thermal ellipsoids set at 50% probability. Selected bond lengths (Å) and angles (deg) associated with the metal center: N1−Pt1 2.061(70), N8−Pt1 1.920(11), N15−Pt1 2.019(14), Pt1−Cl1 2.310(3); N1−Pt1−N8 80.2(5), N8−Pt1−Cl1 178.4(3), N1−Pt1−Cl1 99.5(3), N1−Pt1−N15 161.1(5), N8−Pt1−N15 81.0(5), N15−Pt1−Cl1 99.3(4).

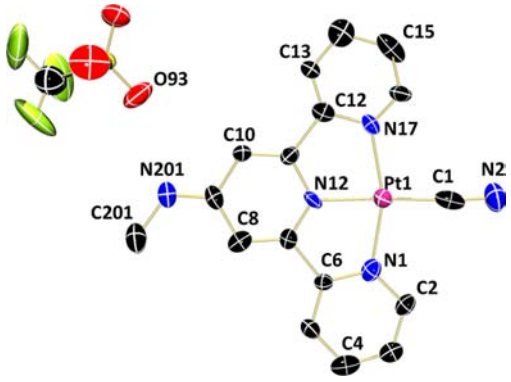

Figure 3. The molecular structure of a representative cation−anion pair of [Pt(ma-T)CN]OTf·MeCN with thermal ellipsoids set at 50% probability. Selected bond lengths (Å) and angles (deg) associated with the metal center: N1−Pt1 2.037(15), N12−Pt1 1.961(12), N17−Pt1 2.090(15), Pt1−C1 1.87(2); C1−N2 1.26(2); N1−Pt1−N12 78.8(5), N12−Pt1−C1 177.1(6), N1−Pt1−C1 98.4(6), N1−Pt1−N17 160.9(5), N12−Pt1−N17 82.1(5), N17−Pt1−C1 100.7(6); N2−C1−Pt1 175.3(15).

the plane that passes through C9, N201, and C201 is 4.1°. Here, the platinum complexes also stack as dimers, but along the *c* axis with a Pt···Pt spacing of 3.67 Å, and the C1−Pt−Pt−C1 torsion angle is 129.08°. Another small difference is that the mean planes through the paired platinum complexes are not quite parallel and intersect at an angle of 1.3°. The distance between N201 of the methylamino group and O93 of the triflate anion is 2.909 Å.

MO Calculations. DFT calculations show that the molecular orbitals of the ground-states generally delocalize over the entire framework, though some orbitals tend to localize in specific domains (Figure 4). For convenience, assume that the axis passing through platinum and the cyanide defines the *x* direction and that the *z* axis is perpendicular to the plane of the trpy ligand. The orbital makeup proves to be very similar in $[Pt(dma\text{-}T)CN]^+$ and $[Pt(ma\text{-}T)CN]^+$. In each case, the 5d(z^2) atomic orbital of platinum effectively defines the HOMO−1. As regards the π orbitals of polypyridine ligands, it is convenient to label them as χ or ψ if they are, respectively, symmetric or antisymmetric with respect to

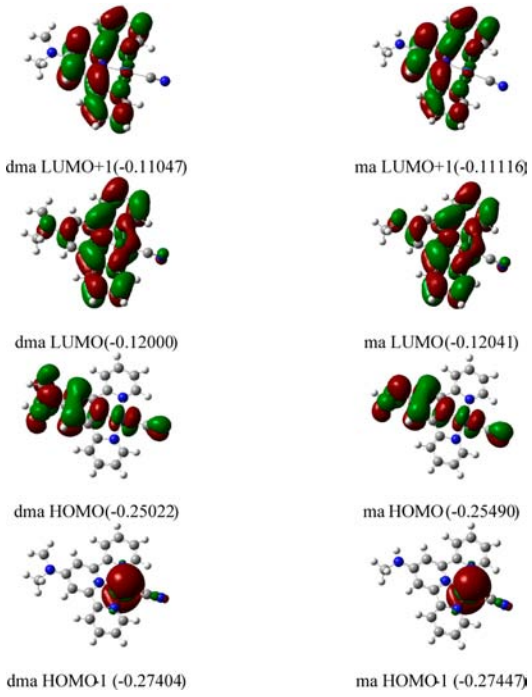

Figure 4. Calculated properties of the frontier molecular orbitals of $[Pt(dma\ T)CN]^+$ (left) and $[Pt(ma\ T)CN]^+$ (right) in S_0 geometries. Energies in parentheses are in au.

rotation about the 2-fold axis that passes through the ligand.[38] Here, the symmetry is only approximate because, for example, the dma group is not exactly in the plane of the trpy ligand; nevertheless, the HOMO of each ligand is essentially a ψ-type orbital. The HOMO mainly localizes on the inner pyridine of the trpy ligand, with significant contributions also coming from the dma nitrogen, the platinum 5d(xz), and the 2p(z) orbital of the cyanide nitrogen. The LUMO also has ψ symmetry but largely delocalizes on the outer pyridines of the trpy ligand. The platinum 5d(xz) and 6p(z) orbitals also contribute to the LUMO, consistent with EHMO calculations of Collison et al.[39]

Hill et al. have also rationalized the electrochemistry of platinum(II) terpyridines in terms of platinum 6p(z) participation.[40] The LUMO+1 has χ symmetry, delocalizes over the whole trpy moiety, and includes some platinum 5d(yz) character. The two states selected for geometry optimization were the ground state S_0 and the lowest energy triplet state T_1. Tables 2 and 3 summarize calculated framework contributions to key molecular orbitals of the low-lying singlet and triplet

Table 2. Percentage Contribution of Fragmental AOs in MOs of $[Pt(dma\text{-}T)CN]^+$ and $[Pt(ma\text{-}T)CN]^+$ Complexes in Their S_0 States

complex	fragment	HOMO−1	HOMO	LUMO	LUMO+1
$[Pt(dma\text{-}T)CN]^+$	% Pt	96.3	23.7	5.4	1.7
	% CN	0.6	3.1	0.9	0.0
	% dma	0.0	41.7	5.8	1.1
	% trpy	3.1	31.5	87.9	97.2
$[Pt(ma\text{-}T)CN]^+$	% Pt	96.3	29.8	5.3	1.8
	% CN	0.6	4.1	0.9	0.0
	% ma	0.1	33.3	5.0	0.4
	% trpy	3.0	32.8	88.8	97.8

dx.doi.org/10.1021/ic4004643 | *Inorg. Chem.* 2013, 52, 8476−8482

excited states. See Table S3 for calculated excited-state properties.

Table 3. Percentage Contribution of Fragmental AOs in MOs of the T_1 States of $[Pt(dma\text{-}T)CN]^+$ and $[Pt(ma\text{-}T)CN]^+$ Complexes ($M_S = 1$)

complex	fragment	SOMO1	SOMO2
	% Pt	42.6	4.9
$[Pt(dma\text{-}T)CN]^+$	% CN	1.8	0.7
	% dma	0.7	5.7
	% trpy	54.9	88.7
	% Pt	33.3	4.3
$[Pt(ma\text{-}T)CN]^+$	% CN	1.2	0.6
	% ma	0.2	5.6
	% trpy	65.3	89.5

DISCUSSION

Both ma-T structures described above entail similar face-centered, orthorhombic packing and exhibit unusual, non-head-to-tail stacking of the platinum complexes. Because the X-ray data do not permit resolution of the hydrogen atoms, the geometry at the substituent nitrogen is not entirely certain in either ma-T complex. Nevertheless, it seems clear that the hybridization is effectively sp^2, in keeping with reported structures involving the analogous $[Pt(dma\text{-}T)CN]^+$ and $[Pt(pyrr\text{-}T)CN]^+$ complexes.[12] Also, consistent with a planar substituent, the distance of 2.909 Å between the N201 nitrogen of the methylamino group and oxygen O93 of the triflate anion (shown in Figure 3) is compatible with N−H···O hydrogen-bond formation.[41,42]

CT Absorption and Emission. Due to the energy requirement for the third ionization of platinum, "pure" MLCT absorption is much less likely in polypyridine complexes of platinum(II) by comparison with related Fe(II), Ru(II), or Cu(I) complexes.[2] Accordingly, charge-transfer excitations in platinum complexes typically entail accompanying admixtures of intraligand (ILCT[16,35]) and/or interligand (LLCT[43,44]) character. The CT absorption maxima of the ma-T complexes shift toward lower energies as the coligand ranges from CN to Cl to CCPh, and the same is true for the other trpy derivatives (Table 1). The trend follows the π-donating ability (CN < Cl < CCPh) as revealed by the ionization energies of HCN, HCl, and HCCPh, which range from 13.6 to 12.7 to 8.8 eV, respectively.[45] Alternatively, data from Table 2 and Ji et al. confirm that coligand participation in the HOMO increases from 3.1% to 41.2% to 85% as the coligand changes from CN to Cl to CCPh.[34] Both arguments suggest that the CT excitation shifts toward lower energy as LLCT character becomes more important.

The impact of ILCT character is apparent from the shift of the wavelength of the absorption with a change of the 4′-substituent on the trpy ligand. Consider the $[Pt(4'\text{-}X\text{-}T)CN]^+$ series, where the CT absorption maximum is 383, 395, or 402 nm if the substituent is methylamino, dimethylamino, or pyrrolidinyl, respectively. The greater electron-donating ability of the $-NR_2$ group as compared with the −NHR group registers in the HOMO in that the substituent participation increases from 33.3% to 41.7% with the addition of a second methyl group (Table 2). The pyrrolidinyl group also involves two R groups, but there is experimental evidence that the ring structure further enhances the donor strength.[46] The expectation is, therefore, that as the trpy ligand shifts from ma-T to dma-T to pyrr-T, ILCT character increases and the CT absorption shifts to a longer wavelength.

Variations in orbital parentage similarly affect the emission results, although the energy differences between states tend to be smaller (Table 1). Pauli-exchange effects help shape the electron distribution in the triplet state, and as a result, the unpaired electrons occupy complementary orbitals delocalized to differing degrees over both outer pyridine moieties. (See the SOMO (singly occupied molecular orbital) contours in the Supporting Information, Figures S2 and S3.) One of the SOMOs utilizes the 5d(xz) orbital of platinum, while the other incorporates 5d(yz). It is also evident that orbitals from a −NHMe or $-NMe_2$ substituent make relatively modest contributions to the SOMOs (Table 3). Nevertheless, experimental results reveal that electron-donating moieties impact the emission. The apt comparison is $[Pt(trpy)CN]^+$, which exhibits a 0−0 emission band at 465 nm and accompanying vibronic structure that is diagnostic of $^3\pi-\pi^*$ orbital parentage.[16] In contrast, the emissions from the modified forms found in Table 1 begin at significantly longer wavelengths of 500 nm or beyond. The signals also progressively shift to a longer wavelength as LLCT character increases with a change of coligand (CN < Cl < CCPh). When the coligand is Cl or CN, the emission likewise shifts to a longer wavelength as the electron-donating ability of the 4′-substituent increases (ma-T < dma-T < pyrr-T). LLCT character may dominate when the coligand is CCPh, because the emission spectra maximize at about the same wavelength, irrespective of the 4′-substituent.

Emission Decay. The emission energy is also a key factor influencing the excited state lifetime and emission quantum yield because the state energy impacts important rate processes. Figure 5 shows the pathways that affect the dynamics of the emitting triplet state. Rate constant k_r signifies the formally spin-forbidden radiative process, which is actually partially allowed by virtue of spin−orbit coupling. Of course, any diminution of heavy metal character will weaken spin−orbit coupling and lower the emission quantum yield. Pathway k_n' in Figure 5 accounts for nonradiative decay via a thermally accessible d−d excited state. The k_n' process can be very efficient and is apparently responsible for the absence of measurable emission from many platinum(II) terpyridine complexes, including $[Pt(trpy)Cl]^+$, in fluid solution.[3,11,33,47] This pathway becomes less important when the ligand environment destabilizes the dσ^* metal−ligand antibonding

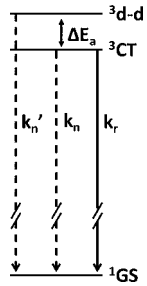

Figure 5. Decay pathways for a platinum(II) polypyridine complex with an emissive CT excited state. Radiationless decay occurs directly to the ground state with rate constant k_n or via a thermally accessible d−d state with rate constant k_n'. The rate constant for the radiative pathway is k_r.

dx.doi.org/10.1021/ic4004643 | Inorg. Chem. 2013, 52, 8476−8482

orbital and elevates the barrier (ΔE_a) against quenching. Direct nonradiative decay to the ground state occurs by the k_n pathway.

Factors that influence k_n include the energy-gap law, which predicts that the rate of nonradiative decay increases exponentially as the energy gap narrows.[48,49] In this limit, high frequency vibrations, such as N−H vibrations, sometimes enhance the rate of nonradiative decay by acting as good acceptor modes in the ground electronic state.[50] Finally, a different effect comes into play if formation of the electronic excited state entails a significant change in the equilibrium geometry, and the assumption of nested potential energy surfaces no longer applies. The coupling to the ground-state surface then becomes much stronger, and the rate of nonradiative decay increases accordingly.[51,52]

All of the decay constants critically depend on the orbital parentage of the emitting state. In particular, studies have shown that introduction of ILCT character has the effect of reducing the rate of thermally activated decay via higher energy d−d states and thereby increasing the excited-state lifetime.[13,34,35] Consistent with this expectation, when the coligand is Cl or CN, the emission shifts to lower energy, and the lifetime increases with the electron-donating ability of the 4′-substituent (ma-T < dma-T < pyrr-T). (A discussion of systems with CCPh as coligand follows below.) Systems based on the ma-T ligand are potentially special cases because the N−H vibration could play an important role in the relaxation process. However, deuteration of the amine group has no measurable effect on the lifetime of [Pt(ma-T)CN]$^+$. In the case of [Pt(ma-T)Cl]$^+$, which has the shortest excited-state lifetime in Table 1, the temperature dependence of the lifetime reveals that a thermally accessible excited state dramatically accelerates radiationless decay. This d−d state occurs some 1830 cm^{-1} above the emitting state. Data in the Supporting Information (Figure S4) reveal that the activation barrier is much higher in [Pt(ma-T)CN]$^+$ due to its relatively strong field coligand. Additional evidence in support of this model comes from the results obtained in a frozen glass at 77 K where population of a higher energy d−d state is no longer feasible (Figure S5). Thus, the principal component observed in the decay of [Pt(ma-T)Cl]$^+$ exhibits a lifetime of 14.8 μs, actually *surpassing* the corresponding lifetime (12.9 μs) observed from [Pt(ma-T)CCPh]$^+$, the ma-T complex that exhibits the longest lifetime in fluid solution (Table 1). Indeed, independent of the 4′-X-T ligand, the lifetime is longer at 77 K with Cl as opposed to CCPh as a coligand, in keeping with expectations based on emission energy considerations.

The three complexes with CCPh as the coligand are noteworthy because they all exhibit microsecond lifetimes at room temperature. The reason is an acetylide coligand naturally enhances the ΔE_a barrier to deactivation in two ways. As a strong σ donor, it drives up the energy of d−d states.[36] At the same time, it introduces LLCT character, which also enhances ΔE_a by lowering the energy of the emitting state.[44] Complementing the CCPh ligand with an amine-substituted 4′-X-T ligand further bolsters the lifetime by introducing ILCT character into the emitting state.[13,34] Accordingly, the room temperature lifetime increases steadily as the donor strength of the substituent builds from methylamino to dimethylamino to pyrrolidinyl. The overall change in lifetime is less than a factor of 2 within the series, however, so relaxation via the d−d state represents a minor pathway for this subset of complexes. The contrast between these systems and [Pt(trpy)CCPh]$^+$ is, however, remarkable. In the absence of an electron-donating group in the 4′-position, the latter complex exhibits a *10-fold* shorter room-temperature, excited-state lifetime.[36]

The lifetime in combination with the emission quantum yield provides an estimate of the radiative rate constant, k_r. Many phenomena contribute to each term, and no simple interpretation explains all the k_r data. Nevertheless, some patterns emerge. The first is that when the coligand is CN, k_r decreases as the terpyridine ranges in the order: ma-T > dma-T > pyrr-T. The explanation may simply be that the emission probability decreases as the excitation becomes more ligand centered.[53] Indeed, the pyrr-T complex always exhibits the smallest k_r value regardless of the coligand (Table 1). Another trend is that the k_r value is always highest when the coligand is Cl. Here, the moderately high atomic number of the chlorine atom and/or its proximity to platinum may account for the elevated k_r values.

CONCLUSIONS

Simple [Pt(4′-X-T)Y]$^+$ complexes rarely exhibit strong emission signals in fluid solution because of strain in the metal−ligand σ bond framework and the availability of thermally accessible d−d excited states that quench potentially emissive excited states. The simple expedient of incorporating a 4′-amine-substituted-terpyridine ligand can dramatically enhance the emission quantum yield by delocalizing the hole away from platinum, introducing ILCT character into the emitting state, and effectively diminishing the role of d−d states. Tuning the amine group is easy as the π-donating strength increases in the order methylamino < dimethylamino < pyrrolidinyl. The results also confirm that incorporating an easily ionized coligand such as CCPh further lowers the energy of the emitting state by introducing LLCT character. However, at some point, direct vibronic coupling to the ground-state energy surface becomes important, because of the energy gap law and/or structural reorganization induced by formal oxidation of the coligand.[2,13,54] Incorporating strong field cyanide as the coligand is usually a more attractive option because it supports higher energy CT emission while still suppressing the influence of d−d states. Thus, within the series investigated, [Pt(pyrr-T)CN]$^+$ exhibits the longest lifetime in fluid solution. The other factor to consider is the radiative rate constant because [Pt(dma-T)CN]$^+$ exhibits almost twice the emission quantum yield, despite having a slightly shorter excited-state lifetime.

ASSOCIATED CONTENT

Supporting Information

Contour plots and density profiles of the SOMOs of the T_1 states of [Pt(dma-T)CN]$^+$ and [Pt(ma-T)CN]$^+$, as well as state energies, along with X-ray data, additional absorption and emission (77 K) data, electrochemical potentials, and temperature dependent studies of emission decay. This material is available free of charge via the Internet at http://pubs.acs.org.

AUTHOR INFORMATION

Corresponding Author

*E-mail: mcmillin@purdue.edu.

Notes

The authors declare no competing financial interest.

dx.doi.org/10.1021/ic4004643 | *Inorg. Chem.* 2013, 52, 8476−8482

■ ACKNOWLEDGMENTS

The NSF funded this research via grants CHE 0847229 (D.R.M.) and CHE 1149968 (A.W.). The authors are grateful to Dr. Tong Ren for the use of electrochemical equipment and to Julia Savchenko for technical assistance. Dr. David Stewart assisted with the double-exponential fits.

■ REFERENCES

(1) Chan, C. W.; Cheng, L. K.; Che, C. M. *Coord. Chem. Rev.* **1994**, *132*, 87−97.
(2) McGuire, R.; McGuire, M. C.; McMillin, D. R. *Coord. Chem. Rev.* **2010**, *254*, 2574−2583.
(3) Eryazici, I.; Moorefield, C. N.; Newkome, G. R. *Chem. Rev.* **2008**, *108*, 1834−1895.
(4) Williams, J. A. G. *Top. Curr. Chem.* **2007**, *281*, 205−268.
(5) Houlding, V. H.; Miskowski, V. M. *Coord. Chem. Rev.* **1991**, *111*, 145−152.
(6) Drew, S. M.; Janzen, D. E.; Buss, C. E.; MacEwan, D. I.; Dublin, K. M.; Mann, K. R. *J. Am. Chem. Soc.* **2001**, *123*, 8414−8415.
(7) Castellano, F. N.; Pomestchenko, I. E.; Shikhova, E.; Hua, F.; Muro, M. L.; Rajapakse, N. *Coord. Chem. Rev.* **2006**, *250*, 1819−1828.
(8) Rivera, E. J.; Barbosa, C.; Torres, R.; Grove, L.; Taylor, S.; Connick, W. B.; Clearfield, A.; Colon, J. L. *J. Mater. Chem.* **2011**, *21*, 15899−15902.
(9) Connick, W. B.; Geiger, D.; Eisenberg, R. *Inorg. Chem.* **1999**, *38*, 3264−3265.
(10) Tears, D. K. C.; McMillin, D. R. *Coord. Chem. Rev.* **2001**, *211*, 195−205.
(11) McMillin, D. R.; Moore, J. J. *Coord. Chem. Rev.* **2002**, *229*, 113−121.
(12) Clark, M. L.; Green, R. L.; Johnson, O. E.; Fanwick, P. E.; McMillin, D. R. *Inorg. Chem.* **2008**, *47*, 9410−9418.
(13) Lazzaro, D. P.; Fanwick, P. E.; McMillin, D. R. *Inorg. Chem.* **2012**, *51*, 10474−10476.
(14) Cho, Y. H.; Park, J. C. *Tetrahedron Lett.* **1997**, *38*, 8331−8334.
(15) Annibale, G.; Pitteri, B.; Wilson, M. H.; McMillin, D. *Inorg. Synth.* **2004**, *34*, 76−81.
(16) Wilson, M. H.; Ledwaba, L. P.; Field, J. S.; McMillin, D. R. *Dalton Trans.* **2005**, 2754−2759.
(17) Yang, Q. Z.; Wu, L. Z.; Wu, Z. X.; Zhang, L. P.; Tung, C. H. *Inorg. Chem.* **2002**, *41*, 5653−5655.
(18) Parker, C. A.; Rees, W. T. *Analyst (Cambridge, U. K.)* **1960**, *85*, 587−600.
(19) Caspar, J. V.; Meyer, T. J. *J. Am. Chem. Soc.* **1983**, *105*, 5583−5590.
(20) Liu, F.; Cunningham, K. L.; Uphues, W.; Fink, G. W.; Schmolt, J.; McMillin, D. R. *Inorg. Chem.* **1995**, *34*, 2015−2018.
(21) Cunningham, K. L.; Hecker, C. R.; McMillin, D. R. *Inorg. Chim. Acta* **1996**, *242*, 143−147.
(22) Sheldrick, G. M. *Acta Crystallogr., Sect. A* **2008**, *64*, 112−122.
(23) Beurskens, P. T.; Beurskens, G.; deGelder, R.; Garcia-Granda, S.; Gould, R. O.; Smits, J. M. M. *The DIRDIF2008 Program System*; Crystallography Laboratory, Univ. of Nijmegen: The Netherlands, 2008.
(24) Becke, A. D. *J. Chem. Phys.* **1993**, *98*, 5648−5652.
(25) Stephens, P. J.; Devlin, F. J.; Chabalowski, C. F.; Frisch, M. J. *J. Phys. Chem.* **1994**, *98*, 11623−11627.
(26) Andrae, D.; Haussermann, U.; Dolg, M.; Stoll, H.; Preuss, H. *Theor. Chim. Acta* **1990**, *77*, 123−141.
(27) Krishnan, R.; Binkley, J. S.; Seeger, R.; Pople, J. A. *J. Chem. Phys.* **1980**, *72*, 650−654.
(28) Cances, E.; Mennucci, B.; Tomasi, J. *J. Chem. Phys.* **1997**, *107*, 3032−3041.
(29) Cossi, M.; Barone, V.; Mennucci, B.; Tomasi, J. *Chem. Phys. Lett.* **1998**, *286*, 253−260.
(30) Mennucci, B.; Tomasi, J. *J. Chem. Phys.* **1997**, *106*, 5151−5158.
(31) Ros, P.; Schuit, G. C. A. *Theor. Chim. Acta* **1966**, *4*, 1−12.
(32) Frisch, M. J.; Trucks, G. W.; Schlegel, H. B.; Scuseria, G. E.; Robb, M. A.; Cheeseman, J. R.; Scalmani, G.; Barone, V.; Mennucci, B.; Petersson, G. A.; Nakatsuji, H.; Caricato, M.; Li, X.; Hratchian, H. P.; Izmaylov, A. F.; Bloino, J.; Zheng, G.; Sonnenberg, J. L.; Hada, M.; Ehara, M.; Toyota, K.; Fukuda, R.; Hasegawa, J.; Ishida, M.; Nakajima, T.; Honda, Y.; Kitao, O.; Nakai, H.; Vreven, T.; Montgomery, J. A., Jr.; Peralta, J. E.; Ogliaro, F.; Bearpark, M.; Heyd, J. J.; Brothers, E.; Kudin, K. N.; Staroverov, V. N.; Kobayashi, R.; Normand, J.; Raghavachari, K.; Rendell, A.; Burant, J. C.; Iyengar, S. S.; Tomasi, J.; Cossi, M.; Rega, N. *Gaussian 09*; Gaussian, Inc.: Wallingford, CT, 2009.
(33) Aldridge, T. K.; Stacy, E. M.; McMillin, D. R. *Inorg. Chem.* **1994**, *33*, 722−727.
(34) Ji, Z. Q.; Azenkeng, A.; Hoffmann, M.; Sun, W. F. *Dalton Trans.* **2009**, 7725−7733.
(35) Crites, D. K.; Cunningham, C. T.; McMillin, D. R. *Inorg. Chim. Acta* **1998**, *273*, 346−353.
(36) Yam, V. W. W.; Tang, R. P. L.; Wong, K. M. C.; Cheung, K. K. *Organometallics* **2001**, *20*, 4476−4482.
(37) Martin, D. S. *Adv. Chem. Ser.* **1974**, 254−275.
(38) Orgel, L. E. *J. Chem. Soc.* **1961**, 3683−3686.
(39) Collison, D.; Mabbs, F. E.; McInnes, E. J. L.; Taylor, K. J.; Welch, A. J.; Yellowlees, L. J. *J. Chem. Soc., Dalton Trans.* **1996**, 329−334.
(40) Hill, M. G.; Bailey, J. A.; Miskowski, V. M.; Gray, H. B. *Inorg. Chem.* **1996**, *35*, 4585−4590.
(41) Zucchi, G.; Scopelliti, R.; Bunzli, J. C. G. *J. Chem. Soc., Dalton Trans.* **2001**, 1975−1985.
(42) Schiessl, W.; Puchta, R.; Bugarcic, Z. D.; Heinemann, F. W.; van Eldik, R. *Eur. J. Inorg. Chem.* **2007**, 1390−1404.
(43) Bevilacqua, J. M.; Eisenberg, R. *Inorg. Chem.* **1994**, *33*, 2913−2923.
(44) Zhou, X.; Zhang, H. X.; Pan, Q. J.; Xia, B. H.; Tang, A. C. *J. Phys. Chem. A* **2005**, *109*, 8809−8818.
(45) Lias, S. G.; Liebman, J. F.; Linstrom, P. J., Mallard, W. G. *NIST Chemistry WebBook, NIST Standard Reference Database Number 69*; National Institute of Standards and Technology: Gathersburg, MD, retrieved January, 2013.
(46) Spivey, A. C.; Arseniyadis, S. *Angew. Chem., Int. Ed.* **2004**, *43*, 5436−5441.
(47) Yip, H. K.; Cheng, L. K.; Cheung, K. K.; Che, C. M. *J. Chem. Soc., Dalton Trans.* **1993**, 2933−2938.
(48) Englman, R.; Jortner, J. *Mol. Phys.* **1970**, *18*, 145−164.
(49) Caspar, J. V.; Kober, E. M.; Sullivan, B. P.; Meyer, T. J. *J. Am. Chem. Soc.* **1982**, *104*, 630−632.
(50) Turro, N. J.; Ramamurthy, V.; Scaiano, J. C. *Principles of Molecular Photochemistry: An Introduction*; University Science Books: Sausalito, CA, 2009.
(51) Gelbart, W. M.; Rice, S. A.; Freed, K. F. *J. Chem. Phys.* **1970**, *52*, 5718−5732.
(52) DeArmond, M. K.; Hillis, J. E. *J. Chem. Phys.* **1971**, *54*, 2247−2253.
(53) A theoretical analysis would depend on higher order calculations involving spin−orbit coupling, which is beyond the scope of this work.
(54) Clark, M. L.; Diring, S.; Retailleau, P.; McMillin, D. R.; Ziessel, R. *Chem.—Eur. J.* **2008**, *14*, 7168−7179.